Proceedings of the 2012 IEEE 12th International Conference on Bioinformatics & Bioengineering (BIBE), Larnaca, Cyprus, 11-13 November 2012

IVUS-based Characterization of Atherosclerotic Plaques using Feature Selection and SVM Classification

Vasilis G. Giannoglou, Dimitris G. Stavrakoudis, and John B. Theocharis
Department of Electrical and Computer Engineering
Aristotle University of Thessaloniki
Thessaloniki, Greece
{vgiannog@auth.gr; jstavrak@auth.gr; theochar@eng.auth.gr}

***Abstract*—In this paper we propose an image-based approach for in-vivo assessment of IVUS images. The method discriminates plaque components into four classes: calcium, necrotic core, fibrous and fibro-fatty. We employ the IVUS frames characterized by virtual histology (VH) for tissue labeling. As a result, we avoid the demerits of visual assessments of observers while at the same time the longitudinal resolution of VH is increased. To describe the textural properties of the tissue classes five different features are extracted from IVUS images. The features are computed by using multiple window sizes so that their values are adapted to the varying heterogeneity of the local patterns. In the next stage, we apply an effective feature selection algorithm on the combined feature space of original features, yielding a small subset of discriminating and non-redundant features. The retained features are used for tissue classification via an SVM classifier. The method is validated against the available VH reference data. The experimental results show that the proposed approach achieves an average accuracy of 81%. This result is obtained by a reduced subset comprising 34 features of the appropriate type and scale of extraction.**

Keywords—Tissue characterization; IVUS images; virtual histology; feature selection; SVM classification

I. INTRODUCTION

Atherosclerotic cardiovascular diseases constitute the major cause of morbidity and mortality in western countries. The great majority of acute ischemic syndromes are attributed to the rupture of vulnerable plaques, which are characterized as lipid-rich necrotic cores surrounded by thin fibrous cap [1]. The propensity of coronary vessels to rupture depends on the proportion of the main tissue components such as calcium, fibrous and lipid core in the plaque area. Therefore, the accurate assessment of plaque composition is an imperative task allowing the physicians to obtain a thorough picture of the disease and design the proper pharmaceutical or interventional therapies.

Intravascular ultrasound (IVUS) is a catheter-based imaging modality that provides a tomographic visualization of coronary vessels. IVUS yields high-resolution cross-sectional images which allow a detailed analysis of artery morphology and its composition. In clinical practice, expert physicians resort to visual assessment of gray-scale IVUS images, i.e., they try to differentiate the various plaque types according to their echogenicity. Nevertheless, several studies indicate that owing to similar textural appearance and spectral overlapping there are severe difficulties in the discrimination between fibrous and fatty as well as calcium and necrotic cores [2]. In addition, manual evaluation is a time consuming process and most importantly, it is subject to inter/intra observer variability. The above shortcomings advocate the use of automated methods for in-vivo plaque analysis from IVUS images.

The variety of tissue characterization techniques suggested in the literature can be divided into three major categories: the image-based approaches [3]-[4], the radio frequency (RF) signal analysis [5] and the combined feature spaces [6]. The image-based methods extract textural features from gray-scale IVUS frames in order to describe the spatial information around pixels. A variety of textural features have been employed in different studies for plaque assessment, including gray-level co-occurrence matrix (GLCM), local binary patterns (LBP), features from run-length matrix (RL) and Gabor filters.

The RF-based methods exploit the spectral content of the backscattered ultrasound RF signals. A prominent paradigm of this category having attracted considerable attention during the past years is the so-called virtual histology (VH) [5]. VH is clinically available for in-vivo plaque assessment and differentiates four tissue components: calcium, necrotic core, fibrous and fibro-fatty. In order to discriminate the various plaques, VH extracts a set of parameters derived from RF spectral shape. The method is validated by histology data, while classification is accomplished using classification trees. Several studies show that VH achieves high classification accuracies and is highly correlated to in-vitro histopathology. Finally, the plaque assessment techniques of the third category devise a combined feature space whereby textural features from reconstructed IVUS images are integrated with spectral features from RF signals.

An important limitation of IVUS-VH emanates from its ECG-gated acquisition. Assuming a pullback speed of 1mm/s and a heart rate of 60 bpm, VH acquires and analyses only one frame/s in one cardiac cycle, located at the peak R-wave. On the other hand, IVUS frames are acquired at a rate of 30 frames/s. This leads to a reduced longitudinal resolution of VH

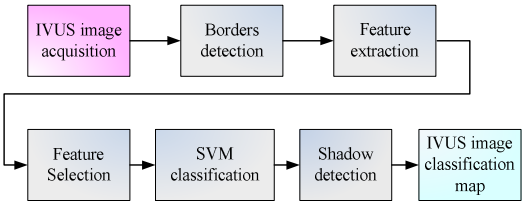

Fig. 1. Block diagram including the processing steps of the proposed tissue characterization method.

and a considerable loss of information at the intermediate frames of the cardiac cycle, where VH color coded maps are not available. In order to increase the longitudinal resolution of VH, an image-based histology (IBH) is suggested in [7]. The method distinguishes plaque components into there classes, namely, calcium, necrotic core and fibro-fatty class. This latter class is obtained by subsuming the fibrous and fibro-lipid patterns into a unique class. The IBH extracts LBP and RL textural features from gray-level IVUS images and handles them individually. Tissue discrimination is attained via SVM classifiers while pattern labels are determined using the associated characterized VH images. The IBH methodology also includes detection of shadow regions and a post-processing section. This section confirms or alters the labels provided by SMV classifier based on some information obtained from gray-level histograms of the IVUS image.

In this paper we suggest an image-based methodology for in-vivo tissue characterization of IVUS images. The basic distinctions and contributions of our approach are outlined as follows:

1) We use the available characterized VH frames to determine the pattern labels of the various plaque components. These patterns are then employed for the classifier's learmning and validation of the method. The use of VH for patterns labeling offers two merits, simultaneously. First, we obtain more reliable plaque assignments derived from RF signal analysis, thus avoiding the interobserver variablity encountered in visual evaluation of plaques. In addition, our method is able to characterize all intermediate IVUS frames within the entire cardiac cycle. Hence, as in IBH, we also retain the asset of increased logitudinal resiolution compared to VH.

2) Contrary to the IBH where the fibrous and fibro-fatty tissue areas are considered as an integrated class, we adhere to the class setup suggested by VH [5]. In particular, the classifier is trained to distinguish plaque components into four classes: calcium (CA), necrotic core (NC), Fibrous (F) and Fibro-fatty (FF). The reason for this choice is that the fibro-fatty tissues are mostly related to heavy lipid accumulations and that lipid–rich core is important ingredient of the thin fibrous cap atheromatic plaques. Thus, detection of fibro-fatty areas is critical for the identification of vulnearable plaques.

3) In order to represent the local structure of patterns effectively, an expanded set of five different textural features is extracted from IVUS images, comprising first order (FO) statistics, GLCM, wavelet features (WF), RLs and LBP. Moreover, each feature is extracted at different scales, i.e., using varying window sizes around pixels. In an attempt to exploit the discrimination power of all features in classifying the different tissue components, we integrate them into a combined feature vector. Usually, the different feature types are treated by other methods individiually [3], while the window size is determined heuristically [4].

4) The combined use of features at multiple windows increases considerably the feature space dimensionality. To cope with this problem our method incorporates a feature selection (FS) mechanism with the goal to select a compact subset of informative and yet non-redundant features, best suited for the discrimination of the different tissue classes. For the needs of this application we suggest the use of the effective SVM-FuzCoC method [8]. The method is a seqenetial forward selection procedure where the relevance of features is qualified by a local evaluation meausre, the so-called fuzzy partition vector (FPV), while the inclusion of new features is decided in terms of fuzzy complementary criterion (FuzCoC). In this context, we propose and analyse two different techniques to determine the fuzzy degrees of patterns to every class: the former uses the principles of fuzzy c-means (FCM) clustering while the latter one is based on the SVM binary classifiers following the one-against-all (OAA) approach.

The rest of the paper is organized as follows. Section II describes the architecture of the proposed algorithm and the feature extraction issue. In section III we present the feature selection algorithm. Section IV outlines the SVM classification and the shadow detection scheme. Section V hosts the experimental results and the paper concludes in section VI with a summary of the proposed method.

II. Proposed IVUS Characterization Method

The block diagram of the suggested image-based plaque assessment algorithm is shown in Fig. 1. Before proceeding to the analysis of plaque composition, we need to determine the lumen-intima and media-adventitia borders of the vessel wall. To achieve this task, we make use of the segmentation method presented in [9], based on textural analysis via a multilevel discrete wavelet frame decomposition. The method does not require manual interventions, although post corrections of the contours are occasionally necessary.

A. Feature Extraction

Textural analyses in IVUS imaging demonstrate that integrating spatial and spectral (gray-level) information improves considerably the classification results. From the wealth of textural features suggested in the literature, we extract in this paper five feature types: FO statistics, GLCM, WF, RL and LBP. The above features are also adopted by other methods, revealing individually their efficacy in tissue characterization [3]-[4].

1) First-Order Staistics: Features derived from FO statistic are fruiful indicators of spatial association. We extract four features of this category, namely, mean (μ), variance (σ^2), skew and kyrtosis.

2) Gray-level co-ocurrence matrix: GLCM features have been extensively used as textural descriptors in image analysis [10]. GLCM estimates the joint probability density function of gray-level pairs and is papameterized by the distance d separating pixel pairs and the orientation angle ϑ of the

neighboring pixels. The distance is set here to $d=1$, while the orientation angle takes four values: $\left[0^o, 45^o, 90^o, 135^o\right]$. From the GLCM elements we compute the following measures: angular second moment (ASM), contrast, homogeneity and shade. For a fixed window size, each of the aforementioned GLCM feature is calculated by averaging over the four different orientations, to assure rotational invariance.

3) Local Binary Patterns: LBP features are used to represent texture patterns into circular neighborhood of radius R that contains P pixels surroubding a central pixel. In our experiments, we calculate three LBP features, namely, *RI* (Rotation-Invariant), *URI* (Uniform Rotation-Invariant), and *VAR* (Local Variance) [11].

4) Run-length features: The RL features strive to capture coarse or finer textural patterns in an image by detecting the gray-level runs appearing along pixel sequences. The texture information is described by the gray-level run-length matrix (GLRLM) $\left[p(i,j)\right]_{M\times N}$, where M is the number of gray levels and N denotes the maximum run length. The entry $p(i, j)$ is defined as the number of runs of length *j* with pixels of gray level *i*. From the GLRLM matrix we extracted eleven RL features emphasizing on various gray-level and/or run lenghts: short run emphasis (SRE), long run emphasis (LRE), gray-level non-uniformity (GLN), run length non-uniformity (RLN), run percentage (RP), low gray-level run emphasis (LGRE), high gray-level run emphasis (HGRE), short run low gray-level emphasis (SRLGE), short run high gray-level emphasis (SRHGE), long run low gray-level emphasis (LRLGE) and long run high gray-level emphasis (LRHGE). For an analytical description of the aforementioned features the reader should refer to [12].

5) Wavelet features: Using a two-channel filter bank, we perform a two-level wavelet decomposition of the original IVUS image using the bio-orthogonal wavelet basis functions. From the tree hierarchy we retain the three subimages created at the first level: horizontal detail (LH_1), vertical detail (HL_1) and the diagonal detail coefficients (HH_1). We also consider the four subimages at the second level created by subsequent decomposition of the approximation LH_1 at the previous level: (LL_2, LH_2, HL_2, HH_2). For each one of the above seven subimages we compute the total energy measure from the associated wavelet coefficients.

In order to capture effectively the varying heterogeneity of plaque components we resort in this paper to a multi-scale feature analysis. In particular, each feature is extracted using multiple windows of six different sizes: 5×5, 7×7, 9×9, 11×11, 13×13, and 15×15. Considering the combinations of the above features and window sizes, we are led to a composite feature set of 175 features (24 FO, 24 GLCM, 42 WF, 66 RL, 18 LBP, gray-level). In order to address the increased feature space dimensionality we apply the FuzCoC-based algorithm on this original feature set. The goal of feature selection is to identify a small subset of powerful and non-redundant features along with their window sizes, most suitable for the differentiation of tissue classes. The incorporation of feature selection has two beneficial effects. First, it reduces the computational burden pertaining to the feature extraction and hence, accelerates the assessment of new IVUS images. Secondly, the consideration of fewer features might improve the generalization capabilities of the classifier.

III. FEATURE SELECTION

The employed FuzCoC-based algorithm is a filter feature selection process that involves three distinct parts: an allocation scheme that assigns fuzzy membership degrees of each pattern to every class, the construction of fuzzy partition vectors (FPV) used for the evaluation of the classification ability of each feature individually, and a selection mechanism to incorporate new informative features.

A. Fuzzy Membership Determination

Let $D=\left\{\left(\boldsymbol{x}_i, c_i\right), i=1,..,N\right\}$ denote a dataset comprising N labeled patterns. $\boldsymbol{x}_i=\left[x_{i,1},...,x_{i,n}\right]^T$ represents the feature vector including a number of n original features ($n=175$), where $x_{i,j}$ denotes the *j*th component of pattern $\boldsymbol{x}_i$. Further, $c_i\in C=\left\{1,...,M\right\}$ are the class labels of patterns and M is the number of information classes ($M=4$).

To assess the discrimination capabilities of each feature, we compare two methods both relying on fuzzy principles. The first one uses a simple allocation scheme resembling to the fuzzy c-means (FCM) clustering. More specifically, considering feature *j,* the fuzzy degree $\mu_k(x_{i,j})\in[0,1]$ to which pattern $x_{i,j}$ belongs to class *k* is computed by applying, once, the following formula:

$$\mu_k(x_{i,j})=\sum_{m=1}^{M}\left[\frac{\left(x_{i,j}-\upsilon_{k,j}\right)^2}{\left(x_{i,j}-\upsilon_{m,j}\right)^2}\right]^{-\frac{1}{b-1}} \tag{1}$$

where

$$\upsilon_{k,j}=\sum_{i\in\mathcal{A}_k}x_{i,j}\Big/N_k \tag{2}$$

is the class *i* mean along the $x_{i,j}$ feature component. $\mathcal{A}_k$ represents the set of indexes of the training patterns belonging to class *k,* N_k is the number of class *k* patterns, and *b* is a fuzzification factor, taken equal to $b=2$ in the experiments. Following (1), the fuzzy memberships are determined according to the distance of pattern $x_{i,j}$ to the class prototypes $\upsilon_{k,j}, k=1,...,M$. Assuming that $x_{i,j}$ is close to $\upsilon_{k,j}$ then $\mu_k(x_{i,j})$ receives a high value (close to 1) while the fuzzy grades apportioned to the other classes are accordingly reduced, and vice-versa. The main asset of the above fuzzy allocation approach comes from its simplicity in the membership calculations, which reduces the computational requirements associated with the FPVs construction.

The second alternative considered here is to use a supervised classification method for the derivation of fuzzy

degrees, and particularly the kernelized fuzzy-output SVM (FO-SVM) [8]. The method involves two stages. Considering the j th feature, a set of M binary SVM classifiers are constructed in the first stage, each one separating a particular class against the rest (OAA). The classifiers are trained using the single dimensional space $x_{i,j}$. The decision scores of the above SVM classifiers are then combined via a suitably devised sigmoidal membership function to compute the fuzzy degrees of patterns to all tissue classes. This method is computationally attractive since SVMs are trained on single features. Nevertheless, it has greater calculation demands compared to the former one, taking into consideration that the SVM complexity increases quadratically with respect to the dataset size.

B. Fuzzy Partition Vectors on Single Features

Initially the patterns of the dataset D are sorted by class labels. Given the pattern ordering, the fuzzy partition vector (FPV) pertaining to feature j is formed by concatenating the membership values of patterns to their target classes:

$$G(j) = \left\{ \mu_G(x_{1,j}), ..., \mu_G(x_{i,j}), ..., \mu_G(x_{N,j}) \right\} \quad (3)$$

FPV is regarded as a fuzzy set defined on the patterns' space, where $\mu_G(x_{i,j})$ denotes the membership value of $x_{i,j}$ to $G(j)$. The membership values are computed from (1), setting index k to the class label where $x_{i,j}$ belongs: $\mu_G(x_{i,j}) = \mu_k(x_{i,j}) \in [0,1]$, $i = 1,...,N$. $G(j)$ serves as a local evaluation metric of feature j with respect to patterns. It allows us to detect the highly classified pattern subsets (large degrees) as well as those patterns that are not adequately covered by this feature individually (lower degrees).

The fuzzy union $G(j) \cup G(q)$ of two FPVs is defined as:

$$\mu_{G(j) \cup G(q)}(x_i) = \max \left\{ \mu_G(x_{i,j}), \mu_G(x_{i,q}) \right\}, \; i = 1,..,N \quad (4)$$

$G(j) \cup G(q)$ indicates the combined discrimination ability of features j and q. The union membership degrees take large values when patterns can be correctly classified either by feature j or q.

The bounded difference $G(q) \text{-} \mid G(j)$ between two FPVs is defined as

$$\mu_{G(q) \text{-} \mid G(j)}(x_i) = \max \left\{ 0, \mu_G(x_{i,q}) - \mu_G(x_{i,j}) \right\} \quad (5)$$

$G(q) \text{-} \mid G(j)$ quantifies the additional contribution provided by feature q in regard to the relevance given by feature j. The FPV difference is used to recognize the excess of evidence offered by a candidate feature on a set of previously selected features.

C. FuzCoC based Fetaure Selection

Feature selection driven by the fuzzy complementary criterion (FuzCoC) is a sequential forward procedure used to select powerful and non-redundant feature subsets suitable for the discrimination of plaque components. Consider a set of initial features, $\mathcal{F} = \left\{ z_1, ..., z_j, ..., z_n \right\}$, $z_j = \left\{ x_{1,j}, ..., x_{i,j}, ..., x_{N,j} \right\}$ where n denotes the total number of features. Following the approach described in section III.B, compute the FPVs, $G(z_j)$, $j = 1,...,n$, associated with each single feature. Let $FS(p)$ denote the set of p features selected up to and including iteration p. The cumulative set $CS(p)$, is an FPV representing the aggregating effect (union) of FPVs of the features contained in $FS(p)$. $CS(p)$ indicates the quality of data coverage achieved by the features already selected at the p-th iteration. Also, assume that z_{ℓ_p} is a candidate feature to be selected at iteration p. $AC(p, \ell_p)$ denotes the additional contribution of z_{ℓ_p} with respect to the cumulative set $CS(p-1)$ obtained at the preceding iteration:

$$AC(p, \ell_p) = \left[CS(p-1) \cup G(z_{\ell_p}) \right] \text{-} \mid CS(p-1) \quad (6)$$

$AC(p, \ell_p)$ represents the excess of membership grades offered by $G(z_{\ell_p})$, compared to the aggregation of the previously selected feature FPVs .

FuzCoC-based feature selection is implemented according to the following steps:

1. ***Initialization***

1.1 Given the feature set $\mathcal{F} = \left\{ z_1, ..., z_j, ..., z_n \right\}$, *compute the feature FPVs* $G(z_j)$, $j = 1,...,n$.

1.2 Set $CS(0) = \varnothing$ *and* $\mathcal{Z} = \varnothing$.

2. ***Select the first feature****: Find feature* z_{ℓ_1} *such that*

$$z_{\ell_1} = \arg\max_{\ell = 1,...,n} \left\{ \left| G(z_\ell) \right| \right\}$$

3.Set $CS(1) = G(z_{\ell_1})$, $\mathcal{Z} \leftarrow \mathcal{Z} + \left\{ z_{\ell_1} \right\}$.

For $p = 2, 3, ...$ *perform the following:*

4. ***FuzCoC –based feature selection***

4.1 Compute the additional contribution of the remaining features

$AC(p, z_j) = G(z_j) \text{-} \mid CS(p-1)$, $j = 1,...,n$, $j \neq \ell_1, ..., \ell_{(p-1)}$

4.2 Find $z_{\ell_p} \in \mathcal{F}$ *such that*

$$\ell_p = \arg\max_{j = 1,...,n} \left\{ \left| AC(p, z_j) \right| \right\} \quad j \neq \ell_1, ..., \ell_{(p-1)}$$

4.2 Calculate the percentage improvement of z_{ℓ_p} *with respect to* $CS(p-1)$*:*

$$h_{\ell_p} = \left(\left| AC(p, z_{\ell_p}) \right| \Big/ \left| CS(p-1) \right| \right) \times 100\%$$

4.3 IF $h_{\ell_p} > e_z$ *THEN*

$$CS(p) = CS(p-1) \cup G(z_{\ell_p}), \; \mathcal{Z} \leftarrow \mathcal{Z} + \left\{ z_{\ell_p} \right\}$$

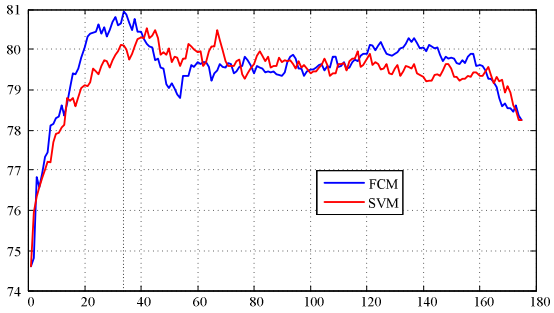

Fig. 2. Overall accuracy versus the number of retained features obtained by applying the feature selection algorithm. The two curves shown correspond to the FCM-based and the FO-SVM method, respectively, used for the FPV construction.

Increment $p \leftarrow p+1$ *and go to step 4.1*

ELSE Terminate FuzCoC at the m-th iteration .

5. ***Output***: *The set* $\mathcal{Z}^* = \{z_{\ell_1}, ..., z_{\ell_m}\}$ *of m selected features.*

At each iteration, the method incorporates those features z_{ℓ_p} that produce the greatest additional contribution $|AC(p, z_j)|$ with respect to the cumulative set $CS(p-1)$ obtained by the existing features in $FS(p-1)$. FuzCoC ensures that the newly incoming feature is complementary, i.e., it provides higher grades for some pattern subsets not adequately covered by the previously selected features. For a detailed description of the method the reader may refer to [8].

IV. SVM Classification

The feature subset retained after applying feature selection is classified via a support vector machine (SVM) classifier [13] following the OAA multi-class strategy. In order to tackle the non-linear relation between the extracted features and tissue classes, we consider an RBF kernel function. For more reliable results, the classifier is evaluated using a 5-fold cross-validation method: the dataset is split into 5 random parts, the 4 of them (80%) are used for SVM learning while the last one (20%) for testing. The reported classification accuracies are averaged over the five folds. The optimal kernel parameters were also obtained through cross-validation and the commonly used grid search approach.

A. Shadow Detection

IVUS gray-scale images often appear with acoustic shadow behind hard plaques (i.e., calcium). However, the color coded maps for shadow areas given by VH may differ from histology assessments, as these results are obtained from backscattered RF signal analysis. When treated on the other hand from a gray-level point of view, they are classified as fibrous or fibro-fatty whereas they should normally be assigned as calcium or necrotic core. To avoid these erroneous misclassifications, the shadow areas are considered as an independent tissue class. Shadow detection is implemented here as post-processing stage operating on the initial classification map obtained by SVM. The IVUS plaque is traversed via a polar sliding sector of small width. At each sector position, we compute the average gray-level value of the part behind calcific regions (to the media-adventitia border) and compare it to a suitably low intensity threshold. If the average intensity is below this threshold, these pixels are reclassified to the shadow class. The detected shadow areas provide a better visualization of the IVUS characterizations, but they are not taken into account in the calculations of the classification accuracies.

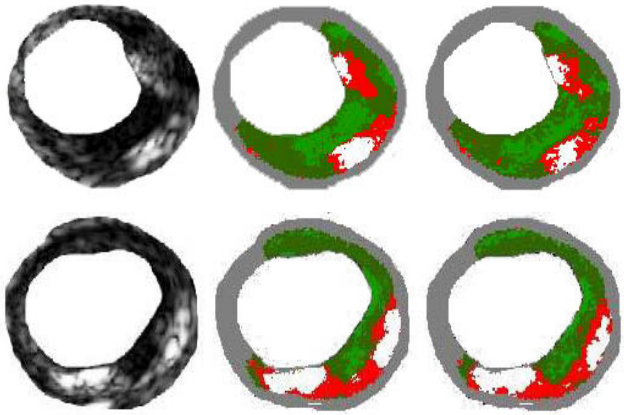

(a) (b) (c)

Fig. 3. Application of our method for two patients (each row of sublots represents a single patient): a) ROI of the IVUS image, b) tissue characterization produced by SVM, and c) IVUS-VH reference image.

V. Experimental Results

The set of IVUS images in these experiments were acquired from 7 patients with known coronary disease. From the image sequences pertaining to each patient, we have collected 5 to 8 vessel sections for further analysis. Following this approach, we are led to 300 frames overall, including the gray-scale IVUS images along with their VH reference frames. After applying IVUS segmentation, from the plaque areas of these frames we have delineated 700 regions of interest (ROIs) of varying size, with their content corresponding to all four plaque classes considered in this study. The pixels contained in the ROIs are labeled using the associated VH characterized frames. Finally, a dataset of 6000 prototypical pixels are collected, comprising the composite feature vector extracted from gray-scale IVUS images and their target labels.

In the next stage, we apply FuzCoC-based feature selection on the original set of 175 features. Fig. 2 shows the overall accuracy (OA) as a function of the selected features for two different methods used for FPV construction: the FCM-based method (1) and FO-SVM. For each feature subset the classification results are obtained by applying the SVM classifier. Furthermore, the reported OAs are averaged over the five different partitions of the dataset. As can be seen from Fig. 2, OA initiates with an adequately high level of 74.6% using the first few selected features and starts increasing almost monotonically for larger feature subsets until a peak performance is achieved. In the following, OA starts to decrease gradually and fluctuates at lower levels of accuracy with the incorporation of additional features. The FCM curve exhibits a sharper rate of increase during the initial phase while at the same time attains a higher OA peak. This indicates that this approach selects quickly more discriminating and complementary features compared to FO-SVM. The design objective is to choose the smallest possible feature subset

TABLE II. AVERAGE SENSITIVITIES (%) AND SPECIFICITIES (%) OBTAINED BY SVM CLASSIFICATION USING THE REDUCED AND THE FULL FEATURE SPACE.

Tissue classes	FCM-based (34 feat.)		FO-SVM (34 feat.)		Full space (175 feat.)	
	Sens. (%)	Spec.(%)	Sens. (%)	Spec.(%)	Sens. (%)	Spec.(%)
Calcium	79.11	95.66	78.56	95.50	73.11	94.34
Necrotic core	84.93	94.07	83.40	93.45	82.53	92.96
Fibrous	83.25	87.67	83.04	87.36	78.71	84.59
Fibro-fatty	72.67	92.39	71.25	91.97	75.83	92.88
AA	79.99	92.45	79.06	92.07	77.55	91.19
OA	80.93		80.10		78.25	

achieving simultaneously the highest classification accuracy. To this end, we retain a subset of 34 features obtained by using the FCM-based FPV construction, which yields an OA of 80.93% in the classification of the four tissue classes considered.

Table II hosts, respectively, the average sensitivities and specificities for each class, separately. The results are shown for three feature subsets used for SVM classification. The first two cases refer to subsets of 34 features selected be FS algorithm using either FCM-based or the FO-SVM methods, respectively, for the construction of FPVs while the third one refers to entire feature vector of 175 features. Table II also provides the OA and the average (per class) accuracies (AA) for each case. Table II indicates that the first case provides the best results in regard to all evaluation metrics ($OA = 80.93\%$). All tissue classes are correctly discriminated with a high level of accuracy. The fibro-fatty class is nevertheless under-estimated to some extent, owing to the spectral overlapping with the fibrous class. Noticeably, this case also exhibits the highest AA value which shows the ability of the SVM classifier to correctly identify patterns of any class, irrespective of the class proportions in the dataset. The second case (FO-SVM) provides slightly inferior results. Contrarily, the accuracies obtained by the full feature space are considerably lower. This underlines the significance of incorporating feature selection, in respect to classification accuracy and reduction of the computational cost required for the analysis of IVUS images. Fig. 3 shows the classification maps obtained by our approach for two representative patients. It can be seen that all plaque components are accurately depicted, as validated by the corresponding VH reference images.

VI. CONCLUSIONS

An image-based methodology is proposed in this paper, for tissue characterization from IVUS images. The suggested technique incorporates the following novelties: a) We use the VH maps for tissue labeling to avoid the interobserver variability in plaque assignments. b) Our method is able to assess all frames of the IVUS sequences thus increasing the longitudinal resolution of VH technology. c) The method differentiates plaque components into four tissue classes which provide a detailed description of IVUS images. d) We devise a combined feature vector by extracting a set of five feature types at multiple window sizes. Most importantly, we apply an effective feature selection method on the original set to reduce feature space dimensionality. Cross-validation against VH reference data shows that our approach achieves a classification accuracy of almost 81 % using a small subset of 34 features of different types and varying window sizes.

REFERENCES

[1] A. P. Burge, A. Farb, G. T. Malcolm, Y. H. Liang, and R. Virmani, "Coronary risk factors and plaque morphology in men with coronary disease who died suddenly," N. Engl. J. Med., vol. 336, no. 18, pp. 1276–1281, May 1997.

[2] N. Gonzalo, H. M. Garcia-Garcia, J. Ligthart, G. Rodriguez-Granillo, E. Meliga, Y. Onuma, J. C. H. Schuurbiers, N. Bruining and P. W. Serruys, "Coronary plaque composition as assessed by greyscale intravascular ultrasound and radiofrequency spectral data analysis," Int. J. Cardiovasc. Imaging, vol. 24, no. 8, pp 811–818, 2008.

[3] O. Pujol, M. Rosales, P. Radeva, and E. Fernandez, "Intravascular ultrasound images vessel characterization using AdaBoost," in Functional Imaging and Modelling of the Hart, ser. Lecture Notes in Computer Science, vol. 2674/2003, pp. 242–251, 2003.

[4] D. G. Vince, K. J. Dixon, R. M. Cothren, and J. F. Cornhill, "Comparison of texture analysis methods for the characterization of coronary plaques in intravascular ultrasound images," Comput. Med. Imaging Graph., vol. 24, no. 4, pp. 221–229, 2000.

[5] A. Nair, B. D. Kuban, E. M. Tuzcu, P. Schoenhagen, S. E. Nissen, and D. G. Vince, "Coronary plaque classification with intravascular ultrasound radiofrequency data analysis", Circulation, vol. 106, pp. 2200–2206, 2002.

[6] S. Escalera, O. Pujol, J. Mauri, and P. Radeva, "Intravascular ultrasound tissue characterization with sub-class error-correcting output codes," J. Sign. Process. Syst., vol. 55, no. 1-3, pp. 35–47, 2009.

[7] A. Taki, H. Hetterich, A. Roodaki, S. K. Setarehdan, G. Unal, J. Rieber, N. Navab, and A. König, "A new approach for improving coronary plaque component analysis based on intravascular ultrasound images," Ultrasound Med. Biol., vol. 36, no. 8, pp. 1245–1258, 2010.

[8] S. E. Moustakidis, G. Mallinis, N. Koutsias, J. B. Theocharis, and V. Petridis, "SVM-based Fuzzy Decision Trees for Classification of High Spatial Resolution Remote Sensing Images," IEEE Trans. Geosci. Remote Sensing, vol. 50, no. 1, pp. 149–169, 2012.

[9] M. Papadogiorgaki, V. Meziaris, Y. S. Chatzizisis, I. Kompatsiaris, and G. D. Giannoglou, "A fully automated texture-based approach for the segmentation of sequential IVUS images," Int. Conf. Syst. Signals Image Process. (IWSSIP), vol. 8, no. 2, pp. 461–464, 2006.

[10] R. M. Haralick, K. Shanmugam, and I. Dinstein, "Textural features for image classification," IEEE Trans. Syst. Man Cybern., vol. 3, no.6, pp. 610–621, 1973.

[11] T. Ojala, M. Pietikainen, and T. Maenpaa, "Multiresolution gray scale and rotation invariant texture classification with local binary patterns," IEEE Trans. Pattern Anal. Mach. Intell., vol. 24, no. 7, pp. 971–987, 2002.

[12] X. Tang, "Texture Information in Run-Length Matrices," IEEE Trans. Image Process., vol. 7, no.11, pp. 1602–1609, 1997.

[13] C. Cortes, and V. Vapnik, "Support vector networks," Mach. Learn., vol. 20, no. 3, pp. 273–297, 1995.